IRIS AperTO

UNIVERSITÀ DEGLI STUDI DI TORINO

AperTO - Archivio Istituzionale Open Access dell'Università di Torino

Statistically optimal fitting of astrometric signals

This is the author's manuscript

Original Citation:

Availability:

This version is available http://hdl.handle.net/2318/140259 since 2015-08-21T12:29:02Z

Published version:

DOI:10.1086/670256

Terms of use:

Open Access

Anyone can freely access the full text of works made available as "Open Access". Works made available under a Creative Commons license can be used according to the terms and conditions of said license. Use of all other works requires consent of the right holder (author or publisher) if not exempted from copyright protection by the applicable law.

(Article begins on next page)

16 October 2026

arXiv:1305.4086v1 [astro-ph.IM] 17 May 2013

Statistically optimal fitting of astrometric signals

M. Gai[1] and D. Busonero[1]
INAF - Osservatorio Astrofisico di Torino, V. Osservatorio 20, 10025 Pino T.se (TO), Italy
gai@oato.inaf.it
and

R. Cancelliere[2]
Università di Torino, Dipartimento di Informatica, C.so Svizzera 185, 10149 Torino, Italy

ABSTRACT

A general purpose fitting model for one-dimensional astrometric signals is developed, building on a maximum likelihood framework, and its performance is evaluated by simulation over a set of realistic image instances. The fit quality is analysed as a function of the number of terms used for signal expansion, and of astrometric error, rather than RMS discrepancy with respect to the input signal. The tuning of the function basis to the statistical characteristics of the signal ensemble is discussed. The fit sensitivity to a priori knowledge of the source spectra is addressed. Some implications of the current results on calibration and data reduction aspects are discussed, in particular with respect to Gaia.

Subject headings: Astrophysical Data — Data Analysis and Techniques

1. Introduction

For efficient extraction of astrometric and photometric information from astronomical data, we often rely on an effective mathematical representation of the signal, suitable to the processing and analysis activities (Mighell 2005). The issue was evidenced e.g. by the attempts at image deconvolution of the initial HST images (Krist & Hasan 1993). The need for modeling the Point Spread Function (PSF) variation, in particular over the large field of view of some modern instruments, leads to different techniques according to specific application needs (Řeřábek & Páta 2008). The dependence of astrometry from source color (i.e. spectral distribution) must be taken into account, even for all reflective optics in space (Le Gall & Saisse 1984; Nemati et al. 2010). Also on ground usage of adaptive optics, which recovers up to a point the diffraction limited performance, requires a detailed model of the PSF for precision measurements (Britton 2006). Modeling and calibration of images for differential astrometry has been addressed from both mathematical and experimental standpoints, demonstrating micro-pixel precision (Chengxing 2011).

In modern spaceborne instruments, with complex telescopes and large area imaging detectors, the instrument response changes over the focal plane, or over the corresponding field of view. The change is due to both optics and detector, related to the geometry and (electro-)optical parameter variation. The effect is both local, modifying the detected signal with respect to the case of diffraction limited images onto an ideal detector, and global, affecting the projection of the focal plane geometry onto the sky. The monochromatic PSF variation is usually attributed to the optical system, described in terms of wavefront error (WFE), and for measurements over a finite bandwidth the signal is weighted by the source spectral distribution. Realistic detector characteristics affect the signal distribution, e.g. because of its geometry and the Modulation Transfer Function (MTF); it is therefore possible to describe the detected signal

shape in terms of an equivalent wavefront, inducing a comparable overall effect. However, detector parameters may have sharp variation over the field, even from pixel to pixel. Besides, field distortion is a large scale effect, introducing smooth variation of the ratio between given small angles on the sky and their projected linear value on the focal plane (e.g. with typical "barrel" or "pincushion" distribution).

Both local and large scale effects can be made acceptably small for many applications by proper design and implementation, but in order to preserve the ultimate measurement performance of an instrument we have to account for them by calibration either on the sky, or through adequate subsystems (e.g. metrology).

This paper deals with the issue of a convenient mathematical representation of the profile variation, over the focal plane and throughout operation, of realistic polychromatic images from a range of objects, in the perspective of a modular approach to data reduction and calibration. For simplicity, we deal with one-dimensional signals; the method can be applied to conventional images e.g. separately along each axis, in principle.

We previously addressed the signal modeling issue, focusing on application to Gaia, in Gai et al. (2010). Here we describe further results of our investigation aimed at strengthening the conceptual framework and improving on specific implementation related aspects. The goal is to define a compact, computationally efficient representation of the signal profile, over finite focal plane regions, suitable to the processing of data from stars spanning a range of magnitude and spectral type. Therefore, the fit optimization is statistical, i.e. focused on collective rather than individual performance.

It is assumed that calibration of field distortion and detector parameter is performed separately from that of the local signal "shape", although in practice the implementation of one module may affect the performance of others. Such issues, therefore, are not discussed in the current work. It may be remarked that at least some detector parameter variations, e.g. smooth changes of MTF and charge transfer efficiency (CTE), may be easily encoded by their effects on the signal profile using the proposed modeling tool.

In our approach, the spatially variant PSF is expanded in a sum of spatially invariant functions, with coefficients varying over the field to describe the instrument response variation for given spectral distribution sources, as in Lauer (2002). The fitting process follows the maximum likelihood approach, with some allowance: on one side, the fit must be compliant with a reasonable range of astrophysical parameter variation among sources; besides, it should be tolerant with respect to instrument response evolution along operations.

In Sec. 2 we deal with the mathematical formulation of an astrometrically sound fitting process, minimizing the photo-center discrepancy between input signal and output fit. This should minimize the systematic errors introduced in applying the fit result as a template, calibrated on a given data set, for location estimate on new data.

Then, in Sec. 3, the fitting functions are defined as an orthogonal set, in order to minimize noise amplification effects and / or correlations in the data reduction results (Makarov et al. 2012).

We evaluate the feasibility and performance of our method by simulation on a study case consistent with the Gaia framework, described in Sec. 4, although the tuning of the fitting method to other applications appears to be straightforward. The approach to calibration of detector and field distortion in Gaia will also be briefly discussed.

The data sets and the fitting algorithm performance are discussed in Sec. 5, evaluating the fit discrepancy with respect to the input signals from the standpoint of photometric and astrometric error as a function of the model parameters. The impact on implementation concerns the number of fitting terms required, within a given range of astrophysical and instrumental parameter variation, and of model related location error.

In Sec. 6 we evaluate the sensitivity of the proposed fit model to the natural variation of spectral distribution among stars. In particular, the location error associated to a given spectral mismatch between the signal template (i.e. the fit result) and new data sets is evaluated. The investigation on fit tolerance to the knowledge of the source effective temperature is relevant to practical implementation within the data reduction system, since it defines the number of different templates required over the whole spectral range to preserve an ade-

quate precision level.

Finally, in Sec. 7, we discuss the potential impact of our results on calibration and implementation aspects, and then we draw our conclusions.

2. Astrometric error of the fit

The detected signal, sampled on K pixels centered on positions x_k, $k = 1, \ldots, K$, is a function $f(x_k - \tau_T)$, located at the "true" photo-center position τ_T, which is the input to the fitting process.

It should be noted that our "signal" is *not* coincident with the readout from the elementary exposure of a single star, even a bright one, but rather the synthetic representation of the instrument response, for a given set of conditions, at very high resolution, as in Guillard et al. (2010). It may be derived from the measured data e.g. by combination of a large set of elementary exposures on a given CCD, in order to achieve a very high signal to noise ratio (SNR) and oversample the instrument response, taking advantage of the natural variation in the relative phase between individual stars and the detector. In practice, the signal used for the fit must have an equivalent noise much below that of any individual exposure (at the μas level or below) to minimize the effects of model errors in its subsequent usage. Residual elementary exposure errors, e.g. from individual background subtraction, are supposed to be reduced by averaging over the whole data set. Also, implementation will require suitable composition rules e.g. for magnitude dependent weighting and consistency check.

Let us assume that $\tilde{f}(x_k)$, i.e. the output of the fitting process, is an approximation of the input function f, with a residual labeled hereafter as the *fit discrepancy* $h(x_k)$:

$$f(x_k - \tau_T) = \tilde{f}(x_k) + h(x_k) \,. \tag{1}$$

It may be noted that a general purpose fit is usually aimed at minimizing the discrepancy $h(x_k)$, e.g. in the least square sense, whereas our goal is to minimize the astrometric error $\delta\tau$ experienced when using the fit result $\tilde{f}(x_k)$ as a template within the location algorithm on new sets of measurements distributed according to f. Although obviously the two requirements coincide in the limit of small errors ($\delta\tau \to 0 \Leftrightarrow h(x_k) \to 0$), the fit with a limited number of terms may have different performance according to either criteria.

In this paper, we address the issue of signal fitting with the focus on minimization of the systematic *astrometric error* or bias.

The Maximum Likelihood photo-center estimate builds on the approach described in Gai et al. (1998), recalled below. The fit discrepancy h can be represented in that framework as a measurement error, introducing a photo-center location error when the optimal location estimate τ_E is searched for by minimization of a weighted square error functional derived from the classical definition of χ^2:

$$\chi^2 = \sum_k \frac{\left[f_k - \tilde{f}_k\right]^2}{\sigma_k^2} \,. \tag{2}$$

The variable dependence here is implicit to simplify the notation: $f(x_k) = f_k$, and so on. The photo-center location estimate is thus independent from the Center Of Gravity (COG) algorithm, which is known to be less than optimal and potentially affected by systematic error, i.e. an astrometric *bias* (Lindegren 1978).

The variance $\sigma^2(x_k)$ associated to the signal distribution f is assumed to be known. It will in general account for several noise sources (signal and background photon statistics, readout noise, dark current, and so on), with the best case limited at the very least by shot noise: $\sigma^2(x_k) \geq f(x_k) \geq 0$ (with all quantities scaled to photons for simplicity).

The location process must find the stationary points of Eq. 2, i.e. solve the equation $\frac{d\chi^2}{d\tau} = 0$, which may be expanded at first order to

$$\sum_k \frac{\left[f_k - \tilde{f}_k\right] f'_k}{\sigma_k^2} = 0 \,, \tag{3}$$

assuming small errors, in particular the astrometric error $\delta\tau = \tau_E - \tau_T$, so that e.g. $f(x_k - \tau_E) \simeq f(x_k - \tau_T)$.

Therefore, taking advantage of the Taylor's expansion of the signal model, i.e. that

$$f(x_k - \tau_E) \simeq f(x_k - \tau_T) - \delta\tau \cdot f'(x_k - \tau_T) \,, \tag{4}$$

we get the location estimate error as

$$\tau_E - \tau_T = -\frac{\sum_k h\left(x_k\right) f'\left(x_k\right)/\sigma_k^2}{\sum_k \left[f'\left(x_k\right)\right]^2/\sigma_k^2}. \quad (5)$$

The location error introduced by the fit may be unbiased, i.e. with zero expected value, under the assumption that the fit discrepancy is itself characterized by zero mean. In general, the correlation between pixels may not be zero, so that the variance estimation of the location error is not trivial. However, it may be remarked that, through Eq. 5, it is possible not only to assess the fit quality by providing an estimate of the astrometric bias introduced by the fitting process, correct from the standpoint of the maximum likelihood approach, but in principle to correct such error as well.

It may be noted that the χ^2 formulation, through Eq. 2, is strictly related to the individual signal distribution.

3. Function basis

The parent function proposed for generation of the monochromatic basis functions is the squared *sinc* function, depending on an adimensional argument related to the focal plane coordinate x, the wavelength λ and the characteristic width L_ξ, as

$$\psi_0^m\left(x\right) = sinc^2\rho = \left[\frac{\sin\rho}{\rho}\right]^2,\ \rho = \pi\frac{xL_\xi}{\lambda F}. \quad (6)$$

This corresponds to the signal generated by a rectangular infinite slit having width L_ξ, in the ideal (aberration free) case of a telescope with effective focal length F. The contribution of finite pixel size, nominal modulation transfer function (MTF) and CCD operation in Time-Delay Integration (TDI) mode are also included. Higher order functions are generated by suitable combinations of the parent function and its derivatives

$$\psi_n^m\left(x\right) = \frac{d}{dx}\psi_{n-1}^m\left(x\right) = \left(\frac{d}{dx}\right)^n \psi_0^m\left(x\right), \quad (7)$$

according to a construction rule ensuring orthonormality by integration over the domain, i.e.

$$\left\langle \psi_p^m\, \psi_q^m \right\rangle = \sum_k \psi_p^m\left(x_k\right)\, \psi_q^m\left(x_k\right) = \delta_{pq}, \quad (8)$$

using the Kronecker's δ notation.

The polychromatic functions are built according to linear superposition of the monochromatic functions, weighted by the normalized detected source spectrum S (which includes the system response), here discretized and indexed by l:

$$\psi_n\left(x\right) = \sum_l S_l\, \psi_n^m\left(x; l\right). \quad (9)$$

Orthogonality is inherited from Eq. 8, due to independence of spatial and spectral variables.

The function basis, similar to that proposed in Gai et al. (2010), is redefined here for minimization of the astrometric error from Sec. 2, so that the fit expansion up to a given term provides a good estimate of the input signal position.

Also, a *common* polychromatic basis is used throughout our investigation. With respect to our previous work, this is more practical for application to the real data reduction, since the basis functions do not need to be generated anew for different spectral type stars. The model will thus be dependent on star colors only through the fit coefficient variation. The polychromatic basis is built for a near solar type source with blackbody spectrum corresponding to temperature $T = 6,000\,K$, which seems to be a reasonable practical trade-off from the results of our previous paper.

3.1. Maximum likelihood fit approach

The fit approach is now cast in a framework similar to that of Sec. 2.

The detected signal $f\left(x_k\right)$ (the photo-center τ is not explicited in the next few steps) is approximated by the fit, represented by the expansion to the order n using the basis functions $\psi_m\left(x_k\right)$:

$$\tilde{f}_n\left(x_k\right) = \sum_{m=0}^{n} c_m\, \psi_m\left(x_k\right). \quad (10)$$

The χ^2 in Eq. 2, taking advantage of Eq. 1, is then a function of the fit error to the same order:

$$\chi_n^2 = \sum_k \frac{h_n^2\left(x_k\right)}{\sigma_k^2}. \quad (11)$$

Taking the signal expansion from order n to order $n+1$, the χ^2 becomes

$$\chi_{n+1}^2 = \chi_n^2 + c_{n+1}^2 \sum_k \frac{\psi_{n+1}^2}{\sigma_k^2} - 2c_{n+1}\sum_k \frac{f\,\psi_{n+1}}{\sigma_k^2}. \quad (12)$$

An ortho-normalization relationship can be imposed on the basis functions, introducing a modification to Eq. 8 such that

$$\langle \psi_m \, \psi_n \rangle = \sum_k \frac{\psi_m \left(x_k\right) \psi_n \left(x_k\right)}{\sigma_k^2} = \delta_{mn} \, . \quad (13)$$

This formulation of scalar product between functions over the domain implicitly gets rid of the sum in the mid term of Eq. 12 (right-hand side).

Then, we define the next expansion coefficient by requiring minimization of the χ^2:

$$\frac{\partial \chi^2}{\partial c_{n+1}} = 0 \, , \quad (14)$$

so that we get

$$c_{n+1} = \sum_k \frac{f \left(x_k\right) \psi_{n+1} \left(x_k\right)}{\sigma_k^2} \, . \quad (15)$$

This expression corresponds to the projection of our input signal f over the basis component ψ_{n+1} using the definition of scalar product from Eq. 13; it simplifies the above expression for χ^2 to

$$\chi^2_{n+1} = \chi^2_n - c^2_{n+1} \, , \quad (16)$$

showing that each additional term effectively contributes to reduction of the fit discrepancy in the maximum likelihood sense. Also, the contribution of each term is limited, since the initial χ^2 is also a limited quantity, thus ensuring the convergence of the fit process.

However, the above formulation must be somewhat mitigated in order to be consistent with different signal instances, e.g. to be able to use a common basis to describe the different signal profiles, e.g. $f^{(r)}$ and $f^{(s)}$, from focal plane positions r and s associated to different instrumental response. The ortho-normalization relationship in Eq. 13 may not be expressed consistently for both signals, since in general $\sigma^{(r)} \neq \sigma^{(s)}$.

Additionally, such formulation is apparently subject to degeneration in the photon limited (PL) case, where the variance equals the signal value in photon units: $\sigma_k^2(PL) = f\left(x_k\right)$. In particular, the denominator and numerator in the coefficient computation (Eq. 15) or similar expressions would cancel out. The degeneration is solved in practice introducing an additional noise term σ^2_{Noise}, taking into account at least the readout noise and the shot noise related to the current background, i.e.

$$\sigma_k^2 = f\left(x_k\right) + \sigma^2_{Noise} \, . \quad (17)$$

However, this variance definition still depends on the individual exposure, i.e. on star magnitude, spectral type, background contribution, and current instrumental response.

Our goal is to define an algorithm for signal fitting suitable to be applied in a straightforward way to a reasonably large set of input signals $\left\{f^{(t)}\left(x_k\right)\right\}$, affected by different perturbations (t).

3.2. Choice of the weight function

The definition related to Eq. 13, although optimal in the maximum likelihood sense with respect to a specific signal instance, associated to variance σ_k^2, is not suited to match *at the same time* different cases within an ensemble of realistic signals, i.e. perturbations to the ideal system. The optimal basis for different signal instances are thus different, due to the dependence on the variance, which is impractical for implementation.

In order to define a convenient common basis for a set of realistic signal instances, a common weight distribution w is adopted to replace the variance σ from Eq. 11 onward, mitigating the stringent requirement related to the maximum likelihood approach, and accepting some degradation with respect to the individual optimal fit. The goal is to achieve a good overall fit performance with a simple common model.

In practice, we use an expression depending on a common reference function F and an additive term p, corresponding to a pedestal applied to the signal, both chosen according to performance on the selected data set:

$$w_k = \frac{F\left(x_k\right) + p}{1 + p} \, . \quad (18)$$

For convenience, F is normalized to unity peak.

It may be noted that the addition of a pedestal to the noiseless signal helps in balancing the relative contribution between the central, high slope region and the side pixels of the signal. Also, the normalization of the weight and reference function are of no consequence onto the astrometric error estimate (Eq. 5), but they do affect the basis normalization (Eq. 13).

The choice of reference function F and of pedestal value p will be discussed in the framework of the simulations below, showing how they can be selected according to a convenient performance trade-off for a given data set.

4. The Gaia study case

Gaia (Perryman 2005; de Bruijne 2012) is the ESA space mission devoted to high precision astrometry, to be launched in 2013. It will perform global astrometric measurements, with a parallax accuracy ranging from a few micro-arcsec (hereafter, μas) to few hundred μas on individual stars, and a few milli-arcsec (hereafter, mas) for some asteroids, in the magnitude range between $V \simeq 8\, mag$ and $V \simeq 20\, mag$. Gaia operates in scanning mode, with continuous observation along a great circle moving over the full sky. It employs two telescopes with primary mirror size $L_\xi \times L_\eta = 1.45 \times 0.5\, m$, separated by a base angle of 106°.5, feeding a large common focal plane, composed of a mosaic of Charge Coupled Device (CCD) detectors operated in Time Delay Integration (TDI) mode.

The Effective Focal Length value $EFL = 35\, m$ corresponds to an optical scale $s = 5".89/mm$: the $10\, \mu m$ detector pixel covers little less than $60\, mas$ on the sky. The Airy diameter of a diffraction limited optical image at a wavelength $\lambda = 600\, nm$ is $2\lambda EFL/L_\xi \simeq 29\, \mu m \simeq 170\, mas$, i.e. of order of three pixels, or somewhat undersampled; the measured image is also affected by the source spectral distribution and realistic detection effects (e.g. MTF and operation). The end-of-mission accuracy goal, resulting from composition of the whole set of measurements, corresponds to a location error of the elementary exposure ranging from a few ten μas for very bright stars to a few mas at the faint end, i.e. from $1/1,000$ to a few $1/100$ of the along scan size of the detector pixel.

The readout mode depends upon the target brightness; binning is applied across scan (low resolution direction), to improve on signal to noise ratio (SNR) and reduce the data volume, for stars fainter than $V \simeq 13\, mag$. The output data is thus a *one-dimensional signal* in the high resolution direction, consistent with our problem formulation. The signal is read out on a limited number of pixels (12 pixels for $13 \lesssim V \lesssim 16\, mag$, six pixels for fainter stars), centered on the signal peak, providing the elementary exposure data. During the data reduction, the individual photo-centers are computed for the whole star sample, thus generating the inputs to the global astrometric solution (Mignard et al 2008).

The data reduction chain (Busonero et al 2010) includes the provisions for calibration based on self-consistency of the set of measurements, so that the instrumental parameters are estimated as well as astrometric and astrophysical parameters. The Gaia design benefits from the built-in differential measurement concept. Many stars are observed subsequently, with a time elapse of less than two hours, by both telescopes, over a limited region of the focal plane, i.e. nearby areas of the same CCDs. The field distortion contributions from either telescope are thus added to the measurements of each star, and may therefore be expected to average out in the repeated coverage of the whole sky. The pixel to pixel variation of CCD parameters is expected to be strongly reduced by TDI operation, thanks to averaging over each column. In practice, field distortion and other instrumental parameters are estimated from the measurements, and data are corrected to provide "clean" individual photo-centers.

It is possible to take advantage of the intrinsic different phase of many individual star observations with respect to the grid of the detector pixel array to retrieve the information on the underlying full resolution signal, i.e. a super-resolution PSF, as in Puschmann (2005). Such synthetic high resolution signal can then be used for a convenient description of the "true" PSF in the data reduction. For convenience, the fit may be defined on "clean" data sets of sources not affected by exceeding peculiarity in their spatial structure, spectral distribution, temporal variability, astrometric behavior, and so on. The derived model can then be used, with proper cautions, for all objects observed, over the same period of time, through the same telescope, on that detector region. The model may also be retained until detection of a significant departure of the instrument response, based on monitoring its consistency with new data.

Our simulations assume usage of such high resolution signals, representing the "true" PSF, as input to the fit in different conditions.

5. Data sets and fit results

The goal of the simulations is to evaluate the practicality and performance of the above conceptual framework by application to different sets of realistic (i.e., not diffraction limited) signals.

The first step of verification is focused on small perturbations, i.e. a set of signal instances affected by limited degradation with respect to the ideal case; the algorithm response can then be expected to be more easily understood. Larger perturbations are introduced in another data set to sample a more realistic range of variation. Hereafter, the two sets will be labeled as SAS and LAS, respectively for "Small" and "Large" Aberration Set; each contains $N = 10,000$ independent signal instances $\left\{ f^{(n)}\left(x_k\right) = f(k;n) \right\}$ $(n = 1, \ldots, N)$.

We generate a set of perturbed images by construction of the optical point spread function (PSF), according to the diffraction integral description (Born & Wolf 1999). The signal perturbations are introduced by means of independent wavefront errors, built by generation of random coefficients applied to Zernike polynomials of the pupil coordinates. The monochromatic PSF is composed with simple source spectra (blackbodies at given temperature) and detection effects (nominal pixel size, MTF and TDI operation; across scan binning) to build the effective detected signal, as in Gai et al. (1998). Such perturbations may represent at first order the effects of other disturbances, e.g. the charge transfer delay in a radiation damaged CCD, also modifying the signal profile.

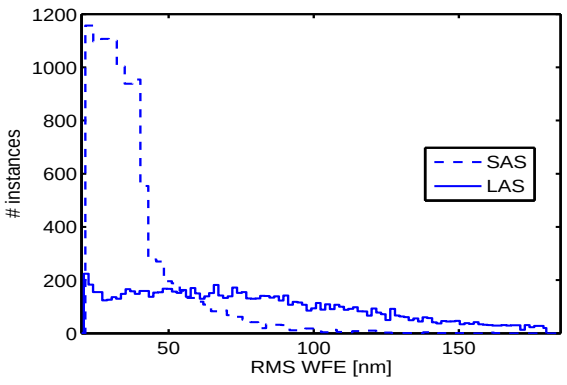

Fig. 1.— Distribution of RMS wavefront error for the two simulation data sets.

The spatial resolution of the simulated signals on the focal plane is $1\,\mu m$ along scan and $3\,\mu m$ across scan, i.e. respectively the high and low resolution coordinates of the instrument. The signal is simulated and analyzed over a range of $\pm 65\,\mu m$, corresponding to 12 ± 0.5 pixels. The pupil sampling is $1\,cm$ in both directions. The simulation is implemented in the Matlab environment. Some key characteristics of the perturbation distribution associated to each data set are summarized in Fig. 1, which shows the RMS WFE histogram for SAS (dashed line) and LAS (solid line), and in Table 1, reporting the RMS WFE mean and standard deviation of both SAS and LAS. The instrument response quality of SAS data corresponds to a degradation of $\sim \lambda/20$ and rarely larger than $\lambda/10$, as expressed in terms of an effective wavelength $\sim 700\,nm$, typical for intermediate type stars observed by Gaia. The LAS data are more evenly spread up to a degradation of $\sim \lambda/4$, roughly corresponding to Rayleigh's criterion for acceptable images.

Each signal instance is generated according to a different random blackbody temperature between $3,000\,K$ and respectively $25,000\,K$ (SAS) and $30,000\,K$ (LAS). The distributions, shown in Fig. 2, do not represent any special stellar population, but are just defined in order to span a reasonable range of spectral types. The spectral resolution is $20\,nm$.

In order to proceed to evaluation of the fit performance on either data set, it is necessary to choose the reference function F defined in Sec. 3.2. The fit algorithm described in Sec. 3.1 is then applied to each signal instance. The fit quality is evaluated in terms of RMS signal discrepancy between input signal and fit, and of mean and RMS astrometric error.
The astrometric error is evaluated for each signal instance according to Eq. 5 in the photon limit.

The former aspect concerns the fit quality in

Table 1: Mean and standard deviation of the RMS wavefront error over each simulation data set.

RMS WFE	Mean [nm]	St. dev. [nm]
SAS	36.12	15.78
LAS	77.72	39.04

the usual sense, whereas the latter two focus on the astrometric quality. The statistics over the data set is discussed as a function of the number of fitting terms and of the pedestal value p, ranging from $p = 0.001$ (which corresponds to attributing negligible weight to the side pixels) to $p = 1$ (signal central lobe weighted twice as much as the wings).

5.1. Fit of SAS

The selected reference function F for the variance is the polychromatic parent function from Eqs. 6 and 9, geometrically scaled by $\sim 6\%$ in order to match approximately the typical RMS width of the signal sample.

The RMS fit discrepancy as a function of the number of fitting terms is shown in Fig. 3, in terms of average (line) and standard deviation (error bar) over the data set for each pedestal value.

The average and RMS astrometric errors as a function of the number of fitting terms are shown respectively in Fig. 4 and Fig. 5.

The fit performance improves in general with increasing number of fitting terms, but the pedestal has opposite effects on photometric and astrometric errors. Increasing pedestal values are associated to increasing photometric errors and decreasing astrometric errors.

The RMS fit discrepancy is smaller for lower pedestal values, and/or for a larger number of fitting terms (which allow for better fitting the signal wings). Very low pedestal values appear to be detrimental to the astrometric performance, since both average and RMS astrometric errors exhibit

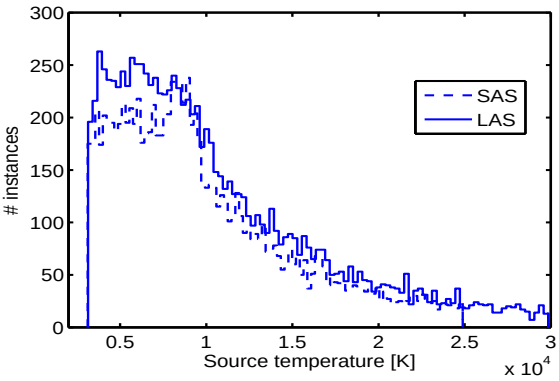

Fig. 2.— Distribution of source temperature for the two simulation data sets.

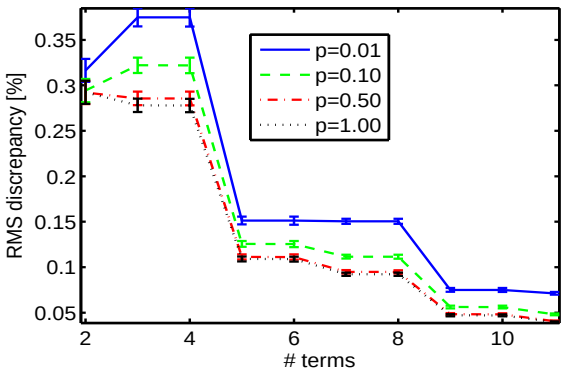

Fig. 3.— Fit RMS discrepancy for SAS; average values (lines) and standard deviation (error bar) over the data set.

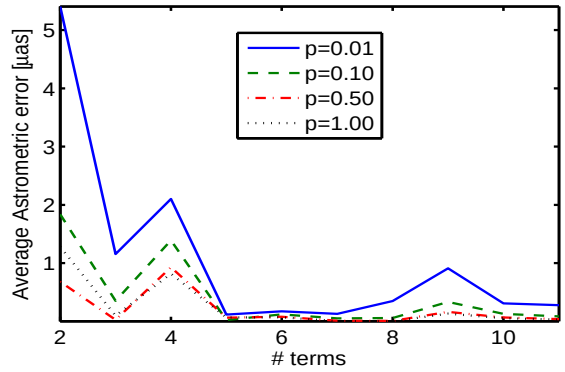

Fig. 4.— Average astrometric error over the SAS data, with pedestal values between 0.01 and one.

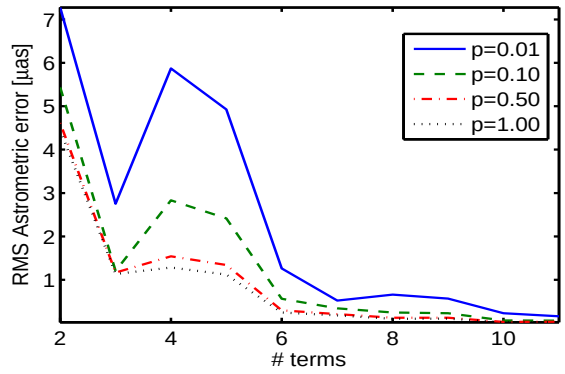

Fig. 5.— RMS astrometric error over the SAS data, with pedestal values between 0.01 and one.

significant fluctuations as a function of the number of fitting terms; larger pedestal values induce more monotonic behaviors. The sub-μas variations for eight terms or more may be related to model limitations.

5.2. Fit of LAS with SAS basis

The selected reference function F for the LAS weight is based on the average $\bar{f}$ of the signal sample $\{f(k;n)\}$,

$$\overline{f}(x_k) = \frac{1}{N}\sum_n f(k;n)\,, \tag{19}$$

using in particular its symmetric component to avoid introducing bias terms through the variance definition:

$$F\,(x) = \frac{1}{2}\left[\overline{f}\,(x) + \overline{f}\,(-x)\right]\,. \tag{20}$$

The selected basis function is the same as for SAS, i.e. derived by ortho-normalization of the non aberrated polychromatic signal and its derivatives, according to Sec. 3.

The RMS fit discrepancy as a function of the number of fitting terms is shown in Fig. 6, again in terms of average (line) and standard deviation (error bar) for each pedestal value.

The average and RMS astrometric errors as a function of the number of fitting terms are shown respectively in Fig. 7 and Fig. 8.

As for the SAS case in Sec. 5.1, the fit performance has a tendency at improving with increasing number of fitting terms, with opposite effects of the pedestal on photometric and astrometric errors. Increasing pedestal values are associated to increasing photometric errors and decreasing astrometric errors. However, both photometric and astrometric errors are significantly larger than in the SAS case, because the larger perturbations require a larger number of fitting terms to account for the signal profile variations. Although it is possible to use the previous simple model for the current case of large signal perturbations, the need for many expansion terms to achieve μas level fitting precision appears to be inconvenient for practical implementation.

5.3. Basis tuning for LAS

The selected reference function is the same as above, but the basis functions are modified to im-

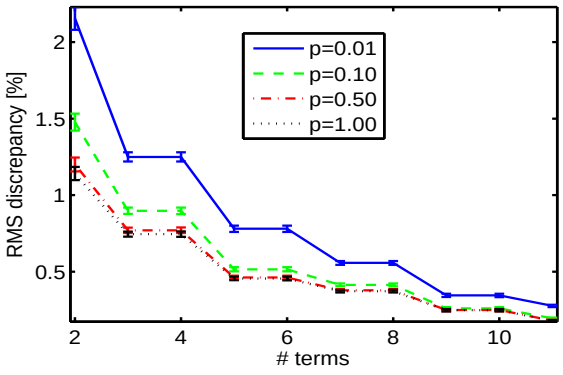

Fig. 6.— Fit RMS discrepancy for LAS, with SAS basis; average (lines) and standard deviation (error bar) over the data.

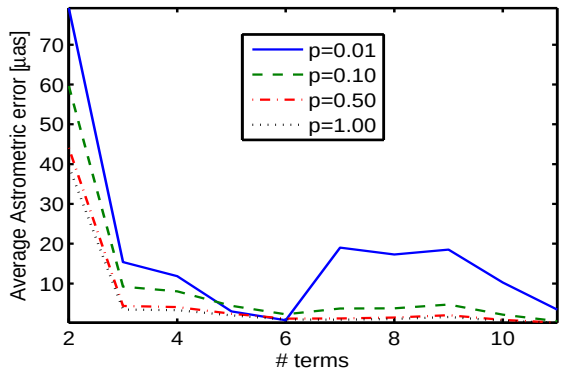

Fig. 7.— Average astrometric error over the LAS data, using the SAS basis.

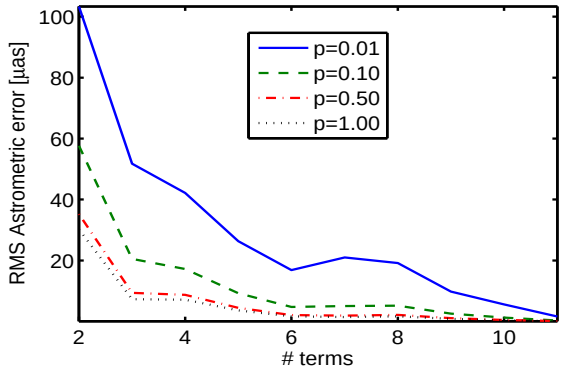

Fig. 8.— RMS astrometric error over the LAS data, using the SAS basis.

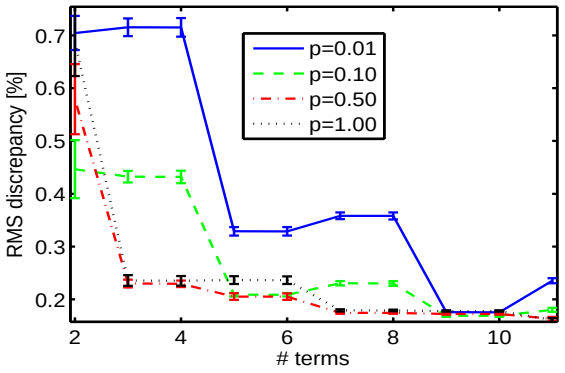

Fig. 9.— Fit RMS discrepancy for LAS, with the modified basis; average (lines) and standard deviation (error bar) over the data.

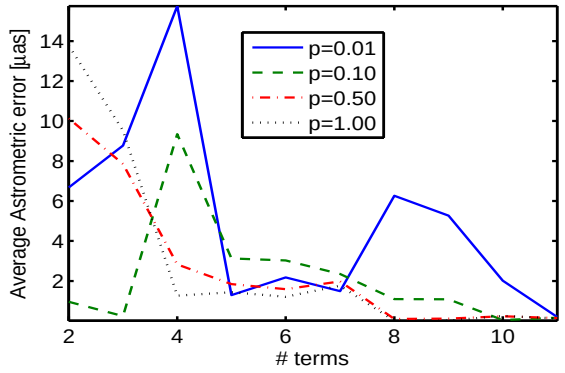

Fig. 10.— Average astrometric error over the LAS data, using the modified basis.

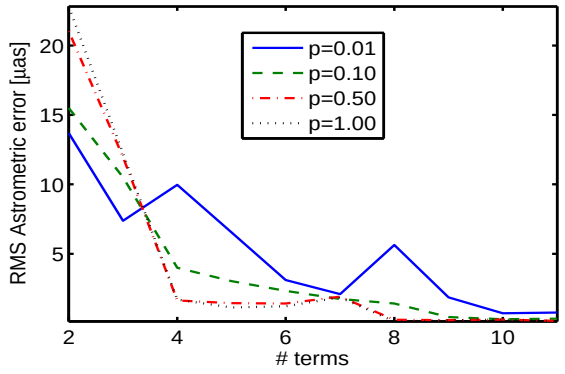

Fig. 11.— RMS astrometric error over the LAS data, using the modified basis.

prove their similarity to typical LAS data. In particular, the parent function becomes the symmetric average signal used above as reference function F for the variance, and the subsequent basis terms are obtained by derivation and ortho-normality according to the prescriptions in Sec. 3. For convenience, the new parent function may be expanded in terms of the SAS basis.

The RMS fit discrepancy as a function of the number of fitting terms is shown in Fig. 9, again in terms of average (line) and standard deviation (error bar) for each pedestal value.

The average and RMS astrometric errors as a function of the number of fitting terms are shown respectively in Fig. 10 and Fig. 11.

The overall trend with number of fitting terms and pedestal value is similar to the previous cases, but the improvement on fit quality achieved by tuning the basis to the data set is significant. The photometric error of the fit drops to values comparable with the SAS case, i.e. RMS fit discrepancy below 0.5% with few fitting terms and intermediate pedestal values. In the same conditions, the astrometric error drops to $< 2\,\mu as$ values.

Modification of the basis according to the current data set characteristics appears therefore to be convenient with respect to the achievable performance, and easily implemented for consistency with the current data.

The two parent functions, i.e. the aberration free polychromatic signal (used for SAS) and the symmetric average signal (used for LAS throughout this section), are shown in Fig. 12, respectively with solid and dashed lines; it may be noted that the change in the function profile is small with respect to the peak value, and it may be described as a low intensity "halo" around the signal central peak, e.g. related to an average symmetric perturbation.

6. Spectral sensitivity

The tolerance to the knowledge of the source effective temperature suggests that a limited number of different templates over the whole spectral range may be sufficient, thus alleviating the requirements of practical implementation within the data reduction system. The fit model performance as a function of the source temperature is a relevant issue, due to the potential

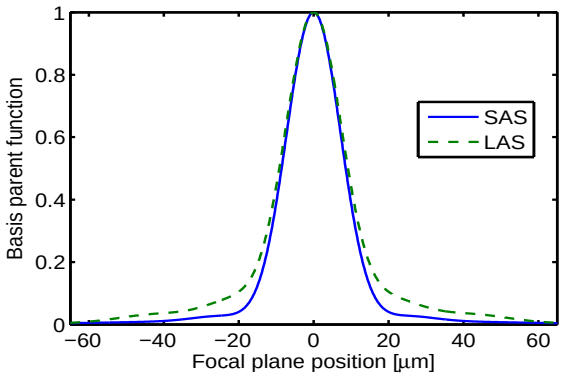

Fig. 12.— Parent functions for SAS (solid line) and LAS (dashed line)

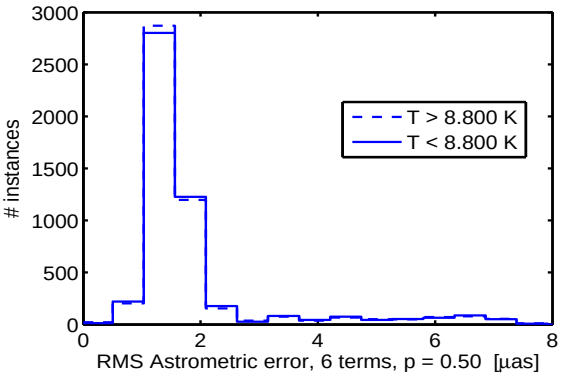

Fig. 13.— Histogram of the fit error distribution for LAS data, using the modified basis, above and below the median source temperature.

risk of chromatic errors (Gai & Cancelliere 2007; Busonero et al. 2006). A preliminary indication on the model sensitivity can be deduced from the results of the previous simulation, e.g. splitting the astrometric error (for a given fitting choice) according to the instance temperature. We select a temperature threshold $T_T = 8,800\,K$, close to the median value of the LAS temperature distribution (solid line in Fig. 2), in order to have a comparable number of instances below and above such value.

We select six terms for the fit, with a pedestal value $p = 0.5$. The results are shown in Fig. 13; the two histograms exhibit negligible difference. The fit errors seem thus to be mostly independent from the source temperature.

In order to check the fit sensitivity to source temperature in more detail, similarly to the case of Sec. 2.2 of our previous paper, we simulate and analyze the data of a subset of 500 perturbations, over the full range of source temperature. Using 20 temperature values, with uniform logarithmic spacing between 3,000 K and 30,000 K, we get a set of 10,000 signal instances, as in Sec. 5, processed in a few hours by our hardware and software system.

The signal perturbation is considered throughout this section as purely optical, and therefore completely described by diffraction; therefore, the variations with the source temperature may be different in practical cases for other kinds of disturbance. In case of perturbations with negligible dependence on the photon wavelength, the current results may thus represent a worst case.

We retain six terms for expansion of the signal fit. The RMS fit discrepancy is practically independent from source temperature. The astrometric error as a function of the source temperature for the first four signal instances of LAS are shown in Fig. 14. The slope variation is typically larger in the effective temperature range associated to near solar and later spectral types, whereas for higher temperatures the curves are smoother.

The collective astrometric error is shown in Fig. 15 vs. source temperature, respectively as mean (solid line) and RMS (dashed line) of the 500 perturbed cases. The mean is basically constant, whereas the RMS features a shallow reduction for near solar type cases, possibly due to the temperature match between the source and the basis (Sec. 3). Both mean and RMS errors are close to the $1\,\mu as$ level, i.e. significantly smaller than the corresponding results of our previous paper. However, by comparison with Fig. 14, the individual variation appears to be significant, suggesting that instrument response is relevant on the μas range, requiring calibration and correction, with moderate requirements on knowledge of the source temperature.

To verify the latter consideration, we simulate and analyze the data of the whole LAS data, upon application of a small variation to the source temperature, respectively $\pm 1\%$ and $\pm 5\%$, similarly to the case of Sec. 2.3 of our previous paper.

This analysis may be relevant to two practical situations, related but not coincident. The former occurs during system calibration, in which

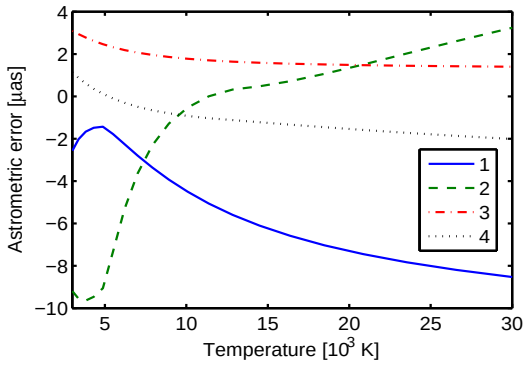

Fig. 14.— Astrometric error as a function of the source temperature for the first four LAS instances.

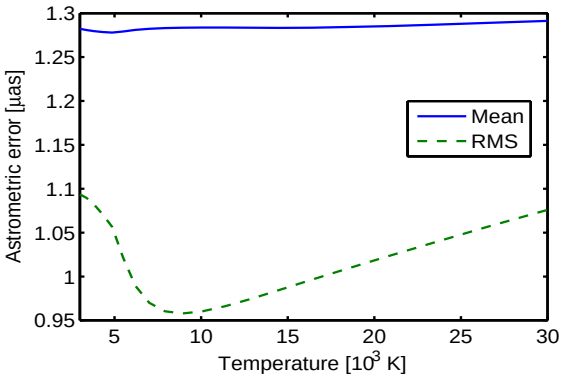

Fig. 15.— Mean (solid line) and RMS (dashed line) astrometric error vs. source temperature, averaged over the first 500 LAS instances.

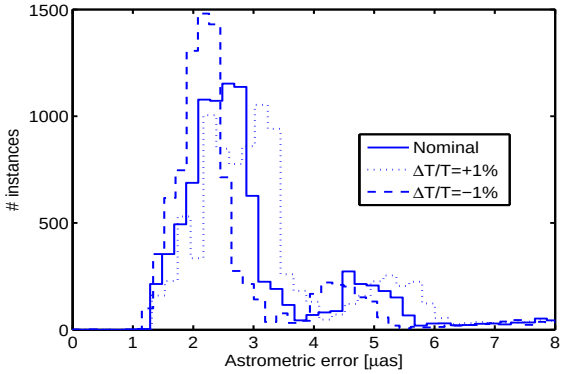

Fig. 16.— Astrometric error on LAS, nominal and with ±1% source temperature error.

the instrument response is being characterized, using the measurements on a set of different stars with similar, but not identical, detected spectrum. The latter concerns data reduction, in which the instrument response representation (encoded into the signal model represented by the fit) is used on all stars within the selected range of spectral types. The simulated model sensitivity can thus be used to select convenient spectral ranges for both computation and application of the signal model.

The spectral distribution discrepancy between the reference signal (associated to the fit on nominal LAS data, limited to six terms) and the data generated with a given source temperature error induces an astrometric error, evaluated according to Eq. 5. As above, the RMS fit discrepancy variation is marginal. In Fig. 16 the distribution of astrometric error associated to the nominal LAS data and ±1% source temperature error is shown. Similarly, the astrometric error distributions related to ±5% source temperature error are shown in Fig. 17. The distributions exhibit a small systematic shift with respect to the nominal case, with the sign correlated to the temperature error.

The mean and standard deviation of the astrometric error associated to the source temperature error is summarized in Table 2. The standard deviation over the sample ranges between 2.41 μas and 2.90 μas, close to the dispersion of nominal data (2.46 μas); besides, the average value of astrometric error appears to be displaced by $\sim 0.3\,\mu\,as$ per each 1% variation in the source tem-

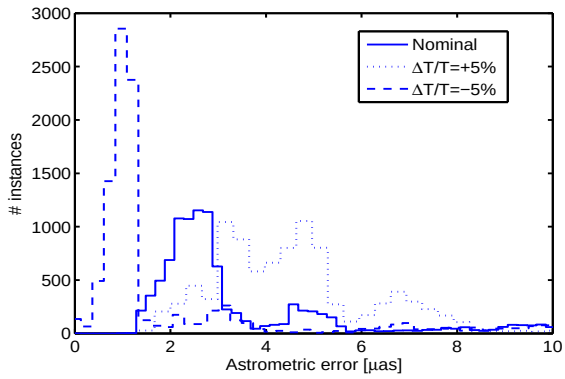

Fig. 17.— Astrometric error on LAS, nominal and with ±5% source temperature error.

Table 2: Mean and standard deviation of astrometric error associated to nominal LAS data and with ±1% and ±5% source temperature error

Astrometric error	Mean [μas]	St. dev. [μas]
Nominal	3.50	2.46
−1%	3.20	2.41
+1%	3.82	2.53
−5%	1.93	2.50
+5%	5.00	2.90

perature.

7. Discussion

The estimate, from Eq. 5, of the systematic astrometric error associated to the fit can be used to advantage in the development of a data reduction pipeline, and above all in providing a straightforward method to assess its behavior. The crucial point is that the bias introduced by the fit can be estimated in a straightforward way, either for introducing corrections in the data reduction, or to support in-depth analysis of the error distribution.

It is not necessary to impose extremely high precision to the fit, e.g. using a large number of terms for expansion of the set of signals, since the error introduced to a given order can be easily assessed, and potentially used to correct the intermediate results. The trade-off can be set by the convenience of retaining limited errors over the whole focal plane, and for a suitably large range of source spectral variation, in order to keep the corrections small.

The bias estimate can be applied to any fitting method, as it is derived from a general maximum likelihood approach. Its application to the basis proposed herein for signal expansion is a special case, in this sense. The performance is good, requiring order of six terms to reduce the RMS error to the μas range over a large set of realistic signals.

The signal profile is potentially different for each detector of a large focal plane, because of the variation on both optical image and device response. In the case of Gaia, it will be different for the two telescopes, at the μas precision level. The signal fit must therefore be defined for at least $7 \times 9 \times 2 = 126$ different profile instances, as many as the number of CCDs in the Gaia astrometric focal plane. A feeling of the implications on calibration and/or monitoring can be achieved in a straightforward way.

The astrometric precision of an elementary exposure of an intermediate magnitude and spectral type star is $\sim 300\,\mu as$. Therefore, in order to assess the instrument response at the $1\,\mu as$ level, i.e. to estimate the best fitting signal profile with such precision, we need to reduce the random error by a factor ~ 300, which requires averaging order of $300^2 \simeq 10^5$ measurements. Any astrometric CCD, with across scan size $\sim 5'$ and scanning rate $\sim 60"/s$, covers one square degree in about 12 minutes. Thus, with an average star density of $\sim 1,000$ stars per square degree, the required number of objects is collected in about 20 hours.

Actual application of the concept requires more detailed analysis, taking into account the real performance and stellar distribution. However, this back-of-the-envelope computation suggests that the science data may indeed be able to provide a self-calibration of the astrometric response of Gaia at the μas level over a one day time scale. Similarly, the response variation across a CCD can be evaluated with comparable precision on a time scale of a few days.

The spectral sensitivity is comparably small, since a ±5% error on the knowledge of the effective source temperature involves an astrometric error of order of $1\,\mu as$, negligible at the elementary exposure level for most stars, and partially averaged in the overall data set due to measurement over different focal plane positions of both telescopes. A set of ~ 20 templates, each computed for a different temperature mean value for a given focal plane position, can therefore provide an acceptable model for the spectral variation of the detected signal. This takes the number of fit instances required to describe the whole astrometric focal plane over the spectral range to $\sim 2,500$. Using a six term expansion, this results in $\sim 15,000$ parameters.

The instrument response variation over the field and with the source spectral type may represent a natural data set (with $\sim 2,500$ instances) for definition of the best basis at a given time. However, the natural evolution of the instrument response during its life will introduce a corresponding variation of the optimal basis. At least two different

strategies may be implemented. On one side, the signal basis may be updated from time to time, using within each period the best set of functions describing the current performance. On the other hand, the full set of measurements can be considered as a unique statistical sample to define the overall best common basis. The latter approach has the benefit of a common signal representation for the whole set of data, potentially at the expense of some increase of the astrometric noise. The impact on overall systematic errors (e.g. regional astrometric errors for the Gaia catalog) may be evaluated by further large scale simulations.

8. Conclusions

We propose an estimate of the fit quality of one-dimensional signals for astrometry, based on a maximum likelihood approach. Building on this framework, and on a simple definition of the function basis, we derive a fitting model easily tailored to a given set of signals. Its performance is evaluated by simulation over a set of realistic signal instances, affected by significant perturbation levels. The fit quality is analyzed as a function of the number of terms used for signal expansion, taking into account not only the RMS discrepancy with respect to the input signal, but above all the astrometric error associated to the fit.

The maximum likelihood fit provides micro-arcsec astrometric errors, and RMS fit discrepancy of a few 0.1%, using six terms. The basis functions can be conveniently tuned to a selected set of signal profiles, e.g. to match the actual instrument response and/or its evolution. The sensitivity to a priori knowledge of the source spectral distribution is low, allowing usage of a limited number of templates.

Some implications on monitoring and calibration of an astrometric instrument using the proposed signal expansion method are discussed, with reference to the typical parameters of Gaia.

The activity is partially supported by the contract ASI I/058/ 10/0. The authors understanding of the subject and its implications benefits from discussions with M. Shao and with M. Lattanzi. The paper clarity significantly improved thanks to the amendments suggested by the referee.

REFERENCES

Born M., Wolf E., 1999, Principles of Optics

Britton M. C., 2006, PASP, 118, 885

Busonero D., Gai M., Gardiol D., Lattanzi M. G., Loreggia D., 2006, A&A, 449, 827

Busonero, D., Gai, M., Lattanzi, M.,G., 2010, SPIE Proc., 7731, 773133-1

Chengxing Z., Shao M., Goulliod R., Nemati B. 2011, MNRAS, 467, 3550

de Bruijne J. H. J., 2012, Ap&SS, online pubblication.

Gai M., Cancelliere R., 2007, MNRAS, 377, 1337

Gai M., Casertano S., Carollo D., Lattanzi M. G., 1998, PASP, 110, 848

Gai M., Cancelliere R., Busonero D., 2010, MNRAS, 406, 2433

Guillard M., et al., 2010, SPIE Proc., 7731, 77310J

Krist J., Hasan H., 1993, A.S.P. Conf. Series, 52, 530

Lauer, T., 2002, SPIE Proc., 4847, 167

Le Gall J. Y., Saisse M., 1984, SPIE Proc., 445, 497

Lindegren L., 1978, in F. V. Prochazka & R. H. Tucker ed., IAU Colloq. 48, 197

Makarov V. V., Veillette, D. R., Hennessy, G. S., Lane, B. F., 2012, PASP, 124, 268

Mighell K. J., 2005, MNRAS, 361, 861

Mignard F., et al., 2008, Proc. of IAU 248, 224

Nemati B. et al., 2010, SPIE Proc., 7734, 77344I

Perryman M. A. C., 2005, in P. K. Seidelmann & A. K. B. Monet ed., Vol. 338 of Astronomical Society of the Pacific Conference Series, 3

Puschmann K. G., Kneer F., 2005, A&A, 436, 373

Řeřábek M., Páta P., 2008, SPIE Proc., 7015, 70152G-1

This 2-column preprint was prepared with the AAS LaTeX macros v5.2.